A Hybrid Islanding Detection Method Based on Pearson Correlation Coefficient

Nusiaba Ali Hassan Hamed[1], George Nyauma Nyakoe[2], Michael Juma Saulo[3]
[1]Dept. of Elec. Eng., Pan African University Institute of Basic Sciences, Technology and Innovation, Juja, Kenya
[2] Dept. of Elec. and Electron. Eng., Jomo Kenyatta University of Agriculture and Technology, Juja, Kenya
3 Department of Engineering and Technology, Technical University of Mombasa, Mombasa, Kenya
Email: ali.nusiaba1@students.jkuat.ac.ke; nyakoe@eng.jkuat.ac.ke; michaelsaulo@tum.ac.ke

***Abstract*—Renewable Energy Resources (RERs) have become essential components in modern electrical power systems. However, one of the significant problems in grid-connected microgrid is unintentional islanding, which can result into outages on the main grid power supply in cases of faults or other uncertainties in the main network. This problem poses a danger to maintenance workers can cause damage to customers and microgrid equipment. Therefore, effective islanding detection methods are necessary to improve the operation of microgrids mitigate and tackle these effects. Previously hybrid proposed islanding detection methods such as the modified reactive power control have only focused on inverter-based sources. This paper proposes a hybrid technique for islanding detection with zero non-detection zone and low impact on power quality. A novel voltage fluctuation injection method based on Pearson correlation coefficient is proposed for islanding detection that involves monitoring the rate of change of Point of Common Coupling (PCC) voltage and switching a high impedance. The Pearson correlation coefficient between the three-phase PCC voltage and the three-phase voltage of switched impedance is used as the islanding detection (ID) index. The proposed method is implemented in a modified IEEE 13-bus test system using MATLAB Simulink. The normally operated grid-connected microgrid had the highest Pearson correlation coefficient. In contrast, the islanding operation had the lowest Pearson correlation coefficient. The method can thus successfully differentiate between islanding and non-islanding events, and islanding can be detected in less than 0.20 s. The proposed method is compared with the islanding detection method based-modified reactive power control (RPC). The proposed method can differentiate between islanding and non-islanding successfully. In contrast, some non-islanding events are incorrectly detected by the RPC-based method.**

***Index Terms*—Islanding detection, islanding fault, Pearson correlation coefficient, periodic switching impedance, voltage fluctuation injection**

I. Introduction

The traditional form of a power system consists of centralized generation, transmission, distribution system, with power flowing only from high to low voltage levels. In contrast, the modern power system is a bi-directional power flow system with distributed generation (DG) sources [1].

Connected DGs are increasing in distributed systems in electrical grids due to the high energy demand and advancements in power-electronic technologies [2]. However, adding DGs in the power system leads to changes in the power system structure from radial structure to looped structure, and reverse power flows are therefore possible [3].

DGs can be found as standalone sources in the distribution networks or interconnected to form a microgrid (MG) to serve specific loads [4].

A microgrid is a small network located at the distribution level of an electrical network consisting of renewable and/or non-renewable energy resources and loads [4]. A microgrid can operate in two modes, either grid-connected mode or islanded model (standalone mode). Both the main grid and microgrid provide power for loads in grid-connected mode. However, only the MG powers the loads in standalone mode [5].

Islanding occurs when the utility grid is disconnected from the microgrid or when the utility power supply is interrupted. Two types of islanding are defined: intentional (refer to scheduled maintenance or economic/management constraints) or unintentional islanding due to faults or other uncertainties in the utility grid. It is also known as inadvertent islanding. Unintentional islanding unwanted phenomenon that threatens power system security damages the network and customer equipment, and can result in the electrocution of utility line workers if care is not taken because some parts of the system can remain energized [6]. Also, unsynchronized circuit breaker reclosing causes large transient currents that can damage the electrical equipment in the utility grid and microgrid. Moreover, islanding can cause ineffective grounding and lead to insulation failure. Consequently, it causes unsafe and severe safety and health hazards [7].

The remaining part of this paper is organized as follows: Section II is the islanding detection methods. Section III highlights the proposed voltage fluctuation injection-based islanding detection. The simulation results and their discussion are presented in section IV. Finally, section V gives the conclusion.

Manuscript received January 15, 2022; revised March 18, 2022; revised again April 8, 2022, accepted April 12, 2022.
Corresponding author: Nusiaba Ali Hassan Hamed (email: ali.nusiaba1@students.jkuat.ac.ke)
This work was supported by African Union Commission (AUC) through PAUSTI research grant.

II. Islanding Detection Methods

The performance indices of islanding detection methods are non-detection zone (NDZ), islanding detection time, false detection ratio, and effect on power quality [8]. Islanding must be detected within 2 s after the disconnection of the main grid according to islanding standards IEEE1547, IEC 62116, and UL1741 [9]. Various islanding detection methods exist. These methods are classified mainly into remote and local islanding detection methods. The local techniques are, in turn, divided into passive, active, and hybrid techniques. The main difference between these techniques is in their way of operation.

Remote islanding detection methods depend on communication between the microgrids and the main grid to detect the islanding situations. These methods are highly reliable, have zero non-detection zones, and have a short detection time with no power quality effect. However, they have expensive and complex implementation. They include power line communication (PLC) method [10], supervisory control and data acquisition method (SCADA) [11], transfer trip method [12], and phasor measurement unit method (PMU) or islanding detection method based on synchronized measurements [13].

Passive islanding detection methods (PIDMs) are based on monitoring parameters such as frequency, voltage, and harmonics distortion. Islanding fault is detected when these parameters exceed their predefined thresholds [5]. These methods used rate of change of voltage (ROCOV), rate of change of frequency (ROCOF) [14], under/over voltage and under/over frequency, rate of change of active power, rate of change of reactive power (ROCORP), and rate of change of phase angle difference [15] for islanding detection. These methods have low cost and easy implementation and do not affect power quality. However, they may have large non-detection zones; reliability is restricted with selected threshold values and is less effective under power generation and demand match [16].

The problems related to passive methods can be mitigated by using intelligent methods like an artificial neural network (ANN), fuzzy logic, decision trees, and adaptive neuro-fuzzy inference systems (ANFIS) [17]. Also, they can be mitigated by signal processing-based methods such as mathematical morphology [18] and Pearson correlation coefficient [19]. Moreover, they can be mitigated by combination of signal processing-based methods and the intelligent based methods [20]–[22] such as combination of wavelet packet transform and binary tree, combination of S transform and ANFIS, combination of discrete wavelet transforms and ANN, and combination of S-transform and ANN.

Active islanding detection methods (AIDMs) depend on introducing a disturbance in the system. This disturbance has a considerable change in parameter values in islanding mode and a slight change in grid-connected mode. As a result, active methods have a small non-detection zone and a low error detection rate. However, these methods can be expensive and complex to implement, have a long detection time, and negatively affect power quality. These methods include impedance measurement, active frequency drift, Sandia voltage shift, and sliding mode frequency shift [23], [24].

Hybrid islanding detection methods (HIDMs) combine PIDMs and AIDMs. First, a passive part is used to predict the occurrence of the islanding fault, and an active method is then used to detect islanding accurately. These methods have a minimal non-detection zone and less power quality than active methods since perturbation is introduced after the islanding suspicion. However, they can have a complex implementation and a long detection time. These methods include unbalanced voltage and frequency set-point, voltage change and power shift, voltage fluctuation injection method, rate of change of reactive power, and load-connecting strategy [25], [26].

A HIDM is proposed by authors of [25]. The method consists of ROCOV as the passive part and rate of change of active power as the active part. At the same time, the authors of [27] proposed a HIDM consisting of ROCOV and ROCORP as passive parts and capacitor switching as an active part. Reza Bakhshi-Jafarabadi and Marjan Popov [28] proposed a HIDM of photovoltaic where ROCOF is a passive part and referenced current disturbance as an active method.

This paper proposes an HIDM that combines ROCOV of PCC voltage as a PIDM and switching high impedance load as an AIDM. The proposed method is tested on a modified IEEE 13-bus system and works by monitoring the ROCOV of PCC voltage and then switching a high impedance as a disturbance to detect islanding. This HIDM considers a grid-connected microgrid with both inverter-based and non-inverter-based sources. The design of the HIDM takes into consideration Zero NDZ and short detection time. The novelty and accuracy of this method arise from the ability of the Pearson correlation coefficient to determine the degree of correlation between the PCC voltage and that of the switched impedance.

III. Proposed Voltage Fluctuation Injection Based Islanding Detection

A HIDM based on the voltage fluctuation injection method is proposed in this paper and implemented for a microgrid with a photovoltaic (PV) array system and a synchronous generator. The proposed technique uses the Pearson correlation coefficient to determine the system is in islanding mode or not. The Pearson correlation coefficient is calculated based on the PCC voltage and the voltage of switched impedance.

A. System Model

The modified IEEE 13-bus test system is chosen to simulate the voltage fluctuation injection method in Simulink-MATLAB. The standard system was modified by the addition of synchronous generator and PV system with nominal voltage of 12 KV. The test data for this work was obtained from [29].The modified IEEE 13-bus test system single line diagram is illustrated in Fig. 1. This figure depicts a microgrid by the dashed line and consists of a PV system at bus 10 and a synchronous

generator at bus 12. Bus 7 is the connection point between the main grid and the microgrid. Table I illustrates DGs, main grid and transformers data, and Table AI and Table AII in Appendix show the lines and the loads data, respectively.

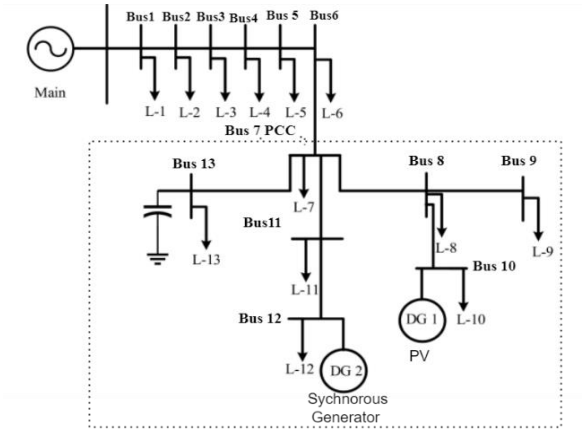

Fig. 1. Modified IEEE 13-bus test system single line diagram.

TABLE I: DGS, MAIN GRID AND TRANSFORMERS DATA

Main Grid	12 kV, 100 MVA, 60 Hz
Solar power array system (DG1)	Cells Per Module 60
	Series-Connected Modules Per String 10
	Parallel Strings 47
	Solar Irradiance 1000 W/m^2
	Operating temperature 25 °C
	Maximum Output Power, 100 KW
Synchronous generator (DG2)	3.125 MW, 60 HZ, 2400V
Transformers	DG1Transformer 500 KVA, 60 HZ 600 V/12 KV YG/YG DG2 Transformer 4 MVA, 60 HZ 2400 V/12 KV YG/YG

B. Determination of Pearson Correlation Coefficient

The correlation between two variables is a measure of the strength of the relationship between them. This association can either be directly or inversely proportional or no association at all. The Pearson correlation is a mathematical tool that measures the linear correlation between two continuous variables using a correlation coefficient [30].

The Pearson Correlation coefficient is used in power system applications such as adaptive protection to analyze and calculate the correlation between uncertain elements and short-circuit measurements [31] and ensure coherency among two different generators [32].

The Pearson correlation coefficient (ρ_{AB}) is calculated as in (1):

$$\rho_{AB} = \frac{\text{cov}(A, B)}{\delta_A \delta_B} \tag{1}$$

where A and B are two variables, cov(A, B) is the covariance of A and B. δ_A and δ_B are the standard deviation of A and standard deviation of B, respectively.

The Pearson correlation coefficient three-phase PCC voltage and three-phase voltage the switched impedance can be calculated using (2) and (3):

$$\rho = \rho_{V_{\text{pcc}}, V_{\text{SW}}} = \frac{\text{cov}\left(V_{\text{pcc}}, V_{\text{sw}}\right)}{\delta_{V_{\text{pcc}}} \delta_{V_{\text{Pert}}}} \tag{2}$$

Compensating the value of $\text{cov}(V_{\text{pcc}}, V_{\text{sw}})$ in (2):

$$\text{cov}\left(V_{\text{pcc}}, V_{\text{sw}}\right) = \frac{1}{n-1}\sum_{i=1}^{n}\left(V_{\text{pcc}_i} - \mu_{V_{\text{pcc}}}\right)\left(V_{\text{sw}_i} - \mu_{V_{\text{sw}}}\right)$$

gives

$$\rho = \frac{1}{n-1}\sum_{i=1}^{n}\frac{\left(V_{\text{pcc}_i} - \mu_{V\text{pcc}}\right)\left(V_{\text{sw}_i} - \mu_{V_{\text{sw}}}\right)}{\delta_{V\text{pcc}}\delta_{V_{\text{sw}}}} \tag{3}$$

where V_{pcc} and V_{sw} are three-phase PCC voltage and three-phase voltage of switched impedance, respectively, and $\mu_{V_{\text{sw}}}$ are the mean of the three-phase PCC voltage and the mean of the three-phase voltage of switched impedance, respectively, $\delta_{V\text{pcc}}$ and $\delta_{V_{\text{sw}}}$ are standard deviations of the three-phase PCC voltage and three-phase voltage of switched impedance respectively, n is number of samples, and i is sample number i of the voltage waveform.

The proposed method calculates the Pearson correlation coefficient between the three-phase PCC voltage and three-phase voltage of the switched impedance using the MATLAB function of the Pearson correlation coefficient given by (4) and (5):

$$\mathbf{R} = \text{corrcoef}\left(V_{\text{pcc}}, V_{\text{sw}}\right) \tag{4}$$

$$\rho = \mathbf{R}(1,2) \tag{5}$$

where **R** is the matrix of correlation coefficients between V_{pcc} and V_{sw}. $R(1, 2)$ is element in the first row and the second column in R matrix which illustrate the cross correlation between V_{pcc} and V_{sw} mentioned in (4). 1 is first row in **R** matrix, and 2 is the second column in **R** matrix.

C. Pearson Correlation Coefficient Application for Islanding Detection

A novel HIDM based voltage fluctuation injection at PCC is proposed in this paper. It starts with monitoring PCC voltage and calculating ROCOV. Islanding is suspected if ROCOV is greater than zero. After islanding suspicion, a periodic impedance is switched at PCC to detect islanding. Then, the Pearson correlation coefficient (ρ) between PCC voltage and the voltage of switched impedance (voltage fluctuation source) is calculated. Islanding is detected by comparing ρ with the Pearson correlation coefficient threshold (ρ_{th}) value.

The Pearson correlation coefficient (ρ) ranges from negative one (−1) to positive one (+1). When ρ is close to positive one, there is a strong positive correlation between V_{pcc} and V_{sw}, but if it is close to negative one, there is a strong negative correlation. If ρ is equal to zero, it means that there is no relationship between V_{pcc} and V_{sw}. From the results, ρ ranges from 0 to 1 and is used as a similarity index. The three-phase PCC voltage and three-

phase voltage of switched impedance and a strong linear correlation in grid-connected mode but the weak linear correlation in islanded mode. So, the value of ρ during grid-connected mode is higher than ρ during islanding.

In other words, variations in PCC voltage due to switching impedance are compensated by the main grid in grid-connected mode. So, the variation in PCC voltage is slight. As a result, ρ in grid-connected mode has a higher value. In contrast, in islanded mode, the variation in PCC voltage due to switching impedance is large because of absent compensation by the main grid. As a result, ρ in islanded mode has a lower value.

ρ_{th} is determined by various simulated islanding and non-islanding case studies. The value of ρ calculated in islanded mode is less than 0.3, while that calculated in grid-connected is higher than 0.3. So, the correlation coefficient threshold is selected to be 0.3.

For a given case study, if ρ in (2) is less than its threshold (ρ_{th}), then the case study represents an islanding event; otherwise, it is a non-islanding event. Fig. 2 illustrates the islanding detection principle. The long of intentional delay is 0.05. This value is determined using the transient cases between the time of starting islanding/non-islanding event and before switching the high impedance load impedance for islanding detection.

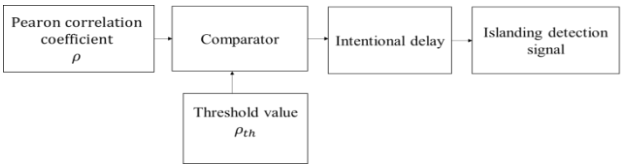

Fig. 2. Block diagram of islanding detection principle.

D. Voltage Fluctuation Source Selection

Voltage fluctuation in a power system occurs due to load changes and distributed generation: the voltage changes caused by intermittent renewable energy sources Furthermore, voltage fluctuation due to switching impedance is one of the crucial features determining changes in the power system conditions [23].

The active part of the voltage fluctuation injection method is done by switching a high impedance load periodically at the PCC. Different 5 MVA impedance load values (resistive-inductive, resistive-capacitive, purely inductive, and purely resistive impedances) have been simulated in MATLAB in grid-connected and islanded modes and the corresponding values of ρ calculated to illustrate the effect of the switching impedance.

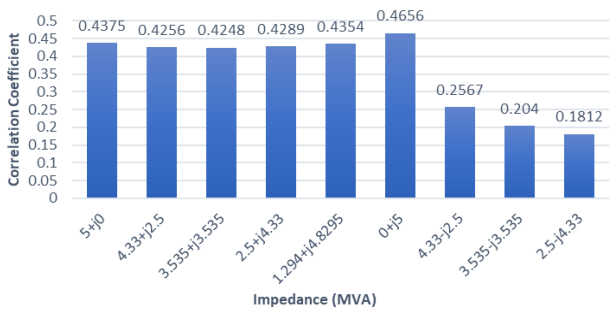

Fig. 3. Correlation coefficient during 5 MVA impedance switching in grid-connected mode.

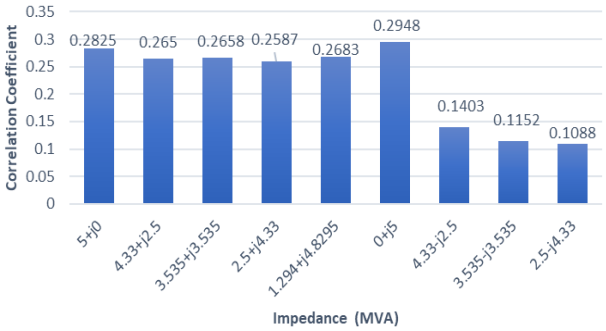

Fig. 4. Correlation coefficient during 5 MVA impedance switching in islanded mode.

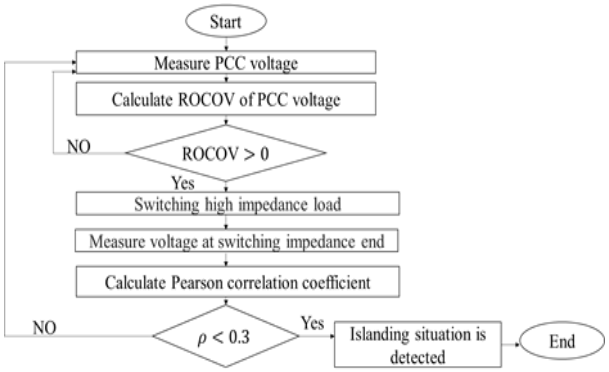

Fig. 5. Flowchart of voltage fluctuation injection method.

Pearson correlation coefficient of a 5 MVA switching impedance during grid-connected mode and islanded modes are shown in Fig. 3 and Fig. 4, respectively. Fig. 3 and Fig. 4 show that a purely inductive load of 5 MVA has the highest value of the Pearson correlation coefficient.

The three-phase PCC voltage and three-phase voltage of switched impedance are measured using separate three phase V-I measurement block. Then the Pearson correlation coefficient between three-phase PCC voltage and three-phase voltage of switched impedance is calculated using (2) through implementing (4) and (5) in MATLAB. Equation (2) is calculated for the three-phase voltage together. The rate of change of voltage is calculated u for phase A through the derivative block and the mean block, to illustrate the effect of islanding and the injection of voltage fluctuation source (switching of high impedance load). The final decision is made by comparing the Pearson correlation coefficient calculated by (5) with its threshold value (0.3) through the relational operator block with less sign.

A flow chart of the voltage fluctuation injection method is shown in Fig. 5. The procedures of the proposed method begin with measuring PCC voltage, calculating ROCOV of PCC voltage, and then switching 5 MVAR pure inductive impedance at PCC when ROCOV is greater than zero. Finally, calculate ρ and detect event as an islanding event if ρ is less than 0.3, otherwise, it will be the non-islanding event.

The proposed method can be implemented in a practical system by measuring the PCC voltage using voltage transformers. Then a digital signal processor

calculates the ROCOV of PCC voltage. When the ROCOV value is greater than zero, a periodic switching signal generator generates a periodic switching command to the high impedance load and measures the voltage at its end. After that, another digital signal processor calculates the Pearson correlation coefficient between the three-phase PCC voltage and the three-phase voltage of switched impedance. This processor decides whether the islanding conditions are met to disconnect the DG.

IV. Simulation Results and Discussion

Various islanding and non-islanding events are implemented in MATLAB – Simulink, which are listed in Table II. All islanding and non-islanding conditions occurred at 0.3 s, and 5 MVAR pure inductive impedance is switched periodically at PCC (bus 7) at 0.35 s with a period of switching equal to 0.04 s.

TABLE II: STUDY CASES FOR THE PROPOSED METHOD AND RPC METHOD

No. Case	Study Case	Pearson Correlation Coefficient (ρ)	Energy Entropy of θ (L2 Norm)
A	Islanding with high power mismatch	0.2911	525.2
B	Islanding DG1	0.2736	507.7
C	Islanding DG2	0.2812	524
D	Capacitor Switching	0.4610	541.9
E	LLL-Fault	0.3237	519.6
F	L-G Fault	0.4323	530.2
G	Islanding with zero power mismatch	0.1138	526.7

The proposed method is compared with the islanding detection method based on modified reactive power control (RPC) [33]. The method is based on the positive sequence of PCC voltage and the phase angle (θ) between the actual and nominal PCC voltage to control the reference reactive power signal. During the normal operation of the grid-connected microgrid, θ is zero; however, it has a considerable value after islanding as illustrated in (6):

$$\theta = (\angle V_{pcc})_{inst} - (\angle V_{pcc})_{nom} \quad (6)$$

where $(V_{pcc})_{nom}$ is nominal PCC voltage, $(V_{pcc})_{inst}$ is actual PCC voltage.

The reactive power reference (Q_{ref}) that is injected into the constant power operation system is given by

$$Q_{ref} = -k_1 \frac{V_{pcc}^{+} - V_N}{V_N} + k_3\theta + Q_{Load} \quad (7)$$

where k_1 and k_3 are constants that are equal to 1 Var and 4 Var, respectively. V_N is the rated of PCC voltage, V_{pcc}^{+} is positive PCC voltage, and Q_{Load} is reactive power of the load.

The islanding index of the RPC method is based on the entropy of discrete wavelet transform coefficients of the phase angle. The method detects islanding by comparing the energy entropy of the voltage phase angle (θ) with its threshold value. The energy entropy of the voltage phase angle (θ) is extracted using discrete wavelet transform (DWT) with the threshold value.

Both methods are implemented on the modified IEEE 13-bus test system shown in Fig. 1. The rate of change of PCC voltage and islanding detection signal are evaluation parameters of the proposed method under different islanding and non-islanding events.

A. Islanding with High Power Mismatch

The islanding mode occurs with high power mismatch condition is implemented by opening the main circuit breaker in the 6-7 line. After the disconnection of the main grid, MG and PCC load form an island, and thus PCC voltage lost its control from the main grid. Thus, the PCC voltage becomes distorted when islanding occurs by opening the main circuit breaker at a time of 0.3 s, as shown in Fig. 6 (a). Also, the distorted voltage fluctuates significantly when 5MVAR impedance is switched periodically from 0.35 s until 0.5 s due to the absence of voltage compensation from the main grid.

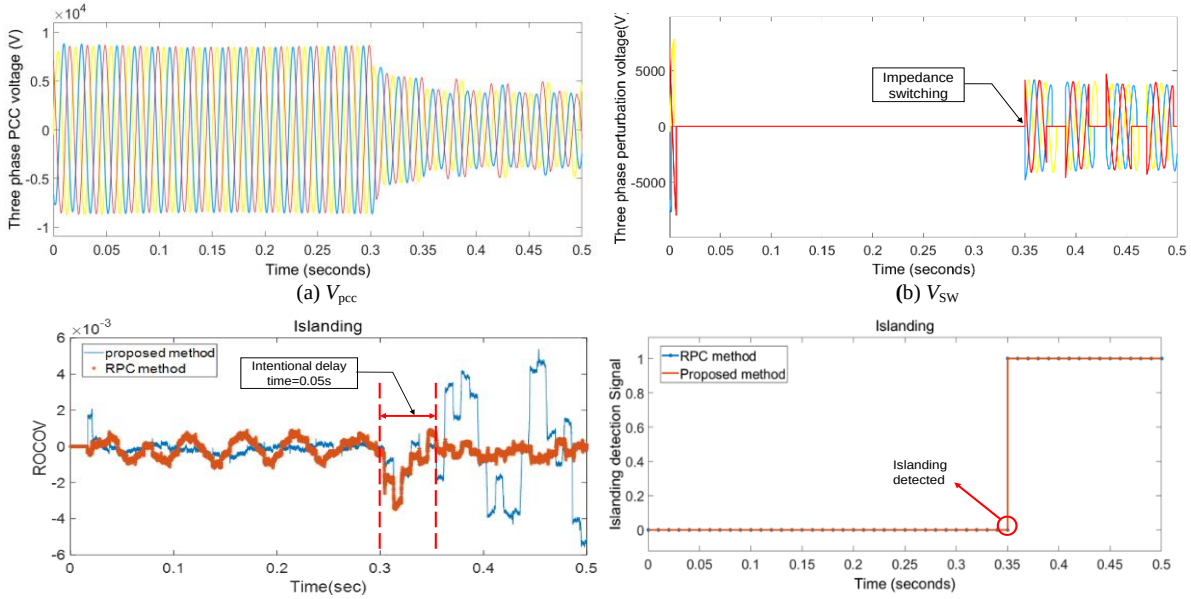

(a) V_{pcc} (b) V_{SW}

(c) ROCOV for the proposed method and RPC method (d) Islanding detection signal

Fig. 6. Waveforms during islanding of microgrid.

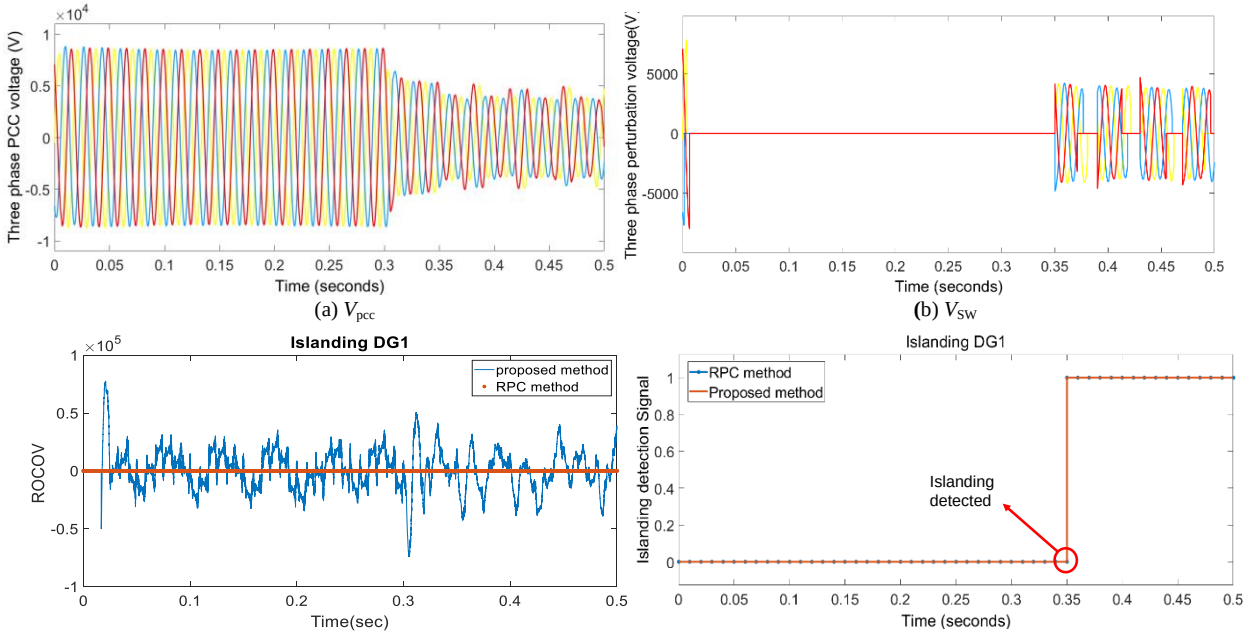

(a) V_{pcc} (b) V_{SW}

(c) ROCOV for the proposed method and RPC method (d) Islanding detection signal

Fig. 7. Waveforms during islanding of DG1.

As shown from Fig. 6 (b), the three-phase voltage of injected impedance is periodic distorted voltage with a magnitude of 5 kV during the islanding from 0.3s to 0.5s.

ROCOV at PCC during islanding is a fluctuated value. The high value of ROCOV demonstrates significant changes in PCC voltage which indicates the islanding. Fig. 6 (c) illustrates the ROCOV of both methods during islanding. The straight line indicates the ROCOV of the proposed method, and the line marked with a star indicates the ROCOV of the RPC method. Islanding occurs at 0.3 s. ROCOV of the proposed method is higher than the ROCOV of the RPC method due to switched impedance. Therefore, the ROCOV of the proposed method illustrates significant changes in PCC voltage better than the ROCOV of the RPC method.

Since the actual value of the PCC voltage during islanding deviates from the nominal PCC voltage, angle θ is used to calculate the reference of the reactive power. Table II shows that the L2 norm for the islanding event is less than 527 (the threshold value of RPC method that proposed in [33]).Therefore, the RPC approach detects islanding accurately. At the same time, the Pearson correlation coefficient is less than 0.3, as shown in Table II. As a result, the suggested method detects islanding correctly. The islanding detection signal for both procedures is equal, as illustrated in Fig. 6 (d).

B. Islanding DG1

Islanding of DG1 (PV system) is implemented by opening the circuit breaker of the line that connects the PV system with the main grid at o.3s.This islanding causes distortions in three-phase PCC voltage, as seen in Fig.7 (a). In addition, there is a distortion in the periodic voltage of injected impedance, as illustrated in Fig. 7 (b).

From Fig. 7 (c) the ROCOV of the proposed method is higher than the ROCOV of the RPC method, which demonstrates the proposed method's effectiveness.

From Table II, the L2 norm of θ for islanding of DG1 is less than 527. As well as the Pearson correlation coefficient ρ is less than 0.3. Thus, as in Fig. 7 (d) both methods determine the islanding of DG1 as an islanding event correctly.

C. Islanding DG2

The islanding DG2 (synchronous generator) occurs by opening the circuit breaker of the line that connects DG2 with the main grid at 0.3s. This islanding causes distortions in three-phase PCC voltage, as seen in Fig. 8 (a). Similar distortion in the periodic voltage of injected impedance as illustrated in Fig. 8 (b) higher than the ROCOV of the RPC method.

From Fig. 8 (c) the ROCOV of the proposed method is higher than the ROCOV of the RPC method, which demonstrates the proposed method's effectiveness.

From Table II, the L2 norm of θ for islanding of DG2 is less than 527. As well as the Pearson correlation coefficient ρ is less than 0.3. Thus, as in Fig. 8 (d) both methods identify islanding of DG2 as an islanding event correctly. The proposed method was able to detect the islanding of DG2 correctly.

D. Capacitor Switching

Capacitor switching in a microgrid is an example of non-islanding events. Between 0.3 s and 0.5 s, a 1.2 MVAr capacitor is connected to bus 13. As a result, PCC voltage slightly increases and fluctuates when 5MVAR impendence is introduced, as shown in Fig. 9 (a). The periodic voltage of injected impedance during capacitor switching with minor distortion is seen in Fig. 9 (b). Fig. 9 (c) shows that the ROCOV of the proposed method has a slightly higher value than the ROCOV of the RPC method. In the RPC method, θ between the actual and nominal PCC voltage due to capacitor switching is used to calculate the reactive power reference. According to Table II, the L2 norm of θ for the capacitor switching is higher than 527. As well as the Pearson correlation coefficient ρ is higher than 0.3. Therefore, the islanding detection signal for both methods equal zero, as seen in Fig. 9 (d).

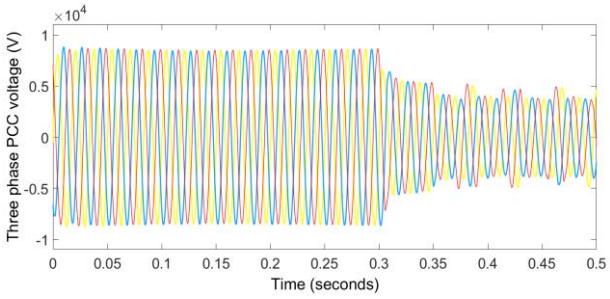

(a) V_{pcc}

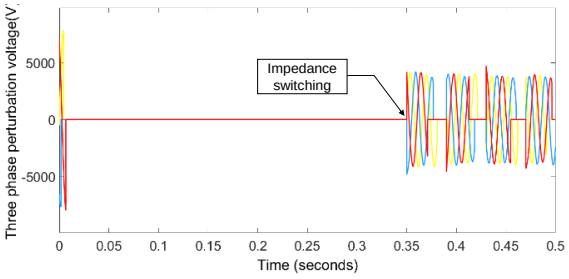

(b) V_{SW}

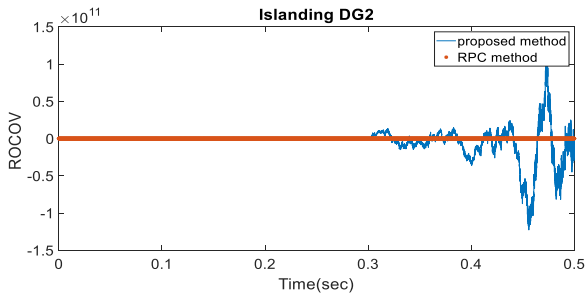

(c) ROCOV for the proposed method and RPC method.

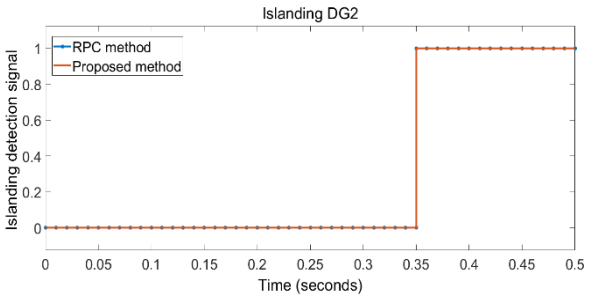

(d) Islanding detection signal

Fig. 8. Waveforms during islanding of DG 2.

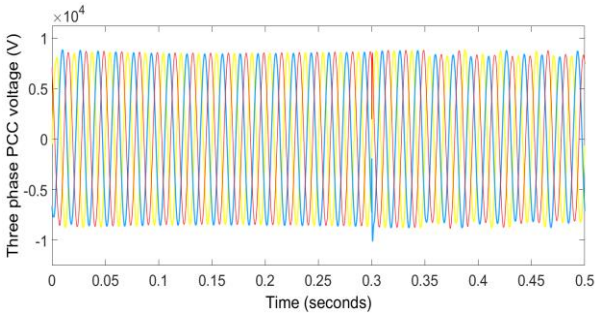

(a) V_{pcc}

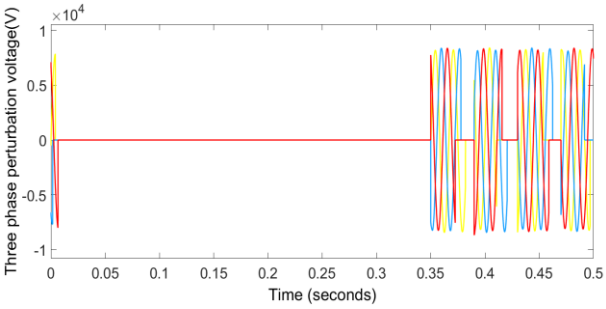

(b) V_{SW}

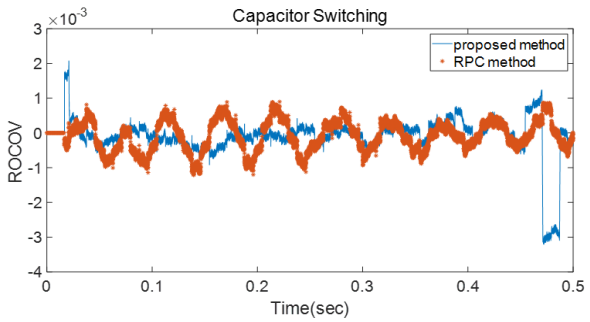

(c) ROCOV for the proposed method and RPC method.

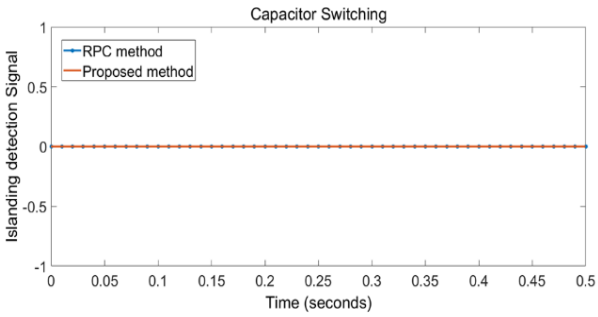

(d) Islanding detection signal for the proposed method and RPC method

Fig. 9. Waveforms during capacitor switching in microgrid.

E. LLL-Fault

A three-phase fault at the microgrid is one non-islanding event. A three-phase short circuit fault was simulated to occur between 0.3 s to 0.5 s on the line between bus 11 and bus 12 with a short circuit resistance equal to 1.5Ω. This fault causes voltage drop and slight distortions in three-phase PCC voltage, as shown in Fig. 10 (a) switched impedance voltage due to LLL- fault is periodic with a magnitude of 5 kV and has slight distortion, as seen in Fig. 10 (b).

Occurrence of a three-phase fault cause distortion in the PCC voltage, which appears significantly at the instance of the fault. After this instance, the ROCOV of the proposed method has a higher value than the ROCOV of the RPC method, as can be seen in Fig.10 (c). There is variation in the actual and nominal PCC voltage in the RPC method during LLL-fault. Therefore, the reactive power reference is accounted for using angle θ.

From Table II, the L2 norm of θ for the LLL fault is less than 527. So, the RPC method detects incorrectly as islanding. In contrast, the Pearson correlation coefficient ρ, according to Table II, is greater than 0.3. So, the proposed method detects LLL fault correctly as a non-islanding event than the RPC method. Therefore, the islanding detection signals for both approaches are seen in Fig.10 (d).

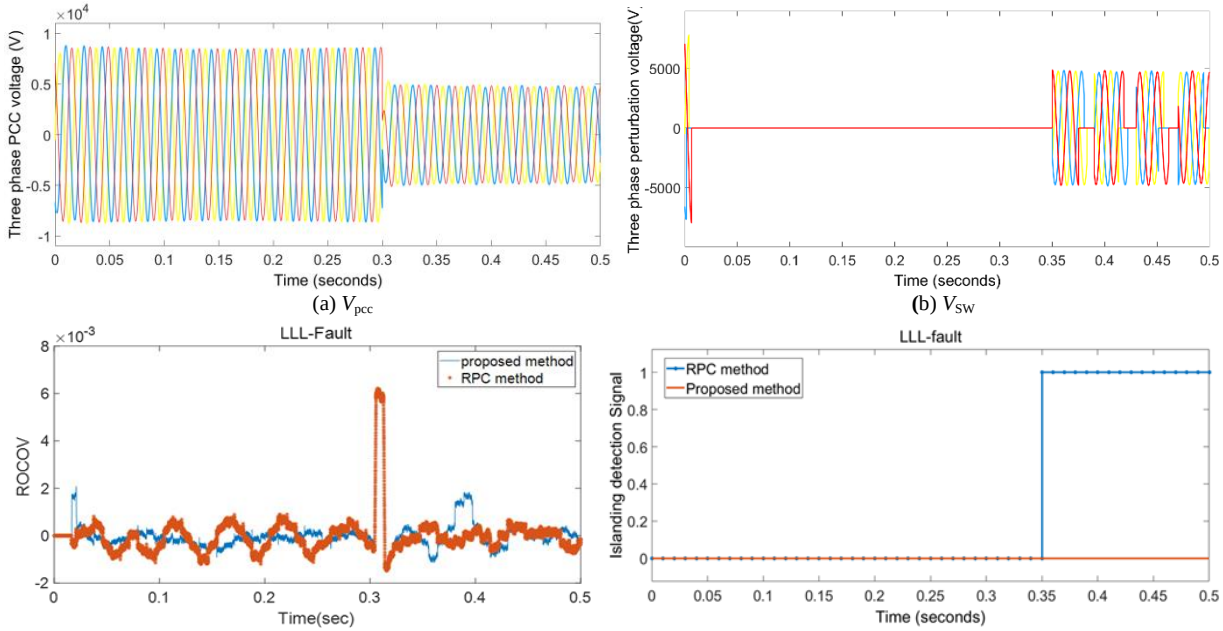

(a) V_{pcc} (b) V_{SW}

(c) ROCOV for the proposed method and RPC method. (d) Islanding detection signal

Fig. 10. Waveforms during LLL- fault in microgrid.

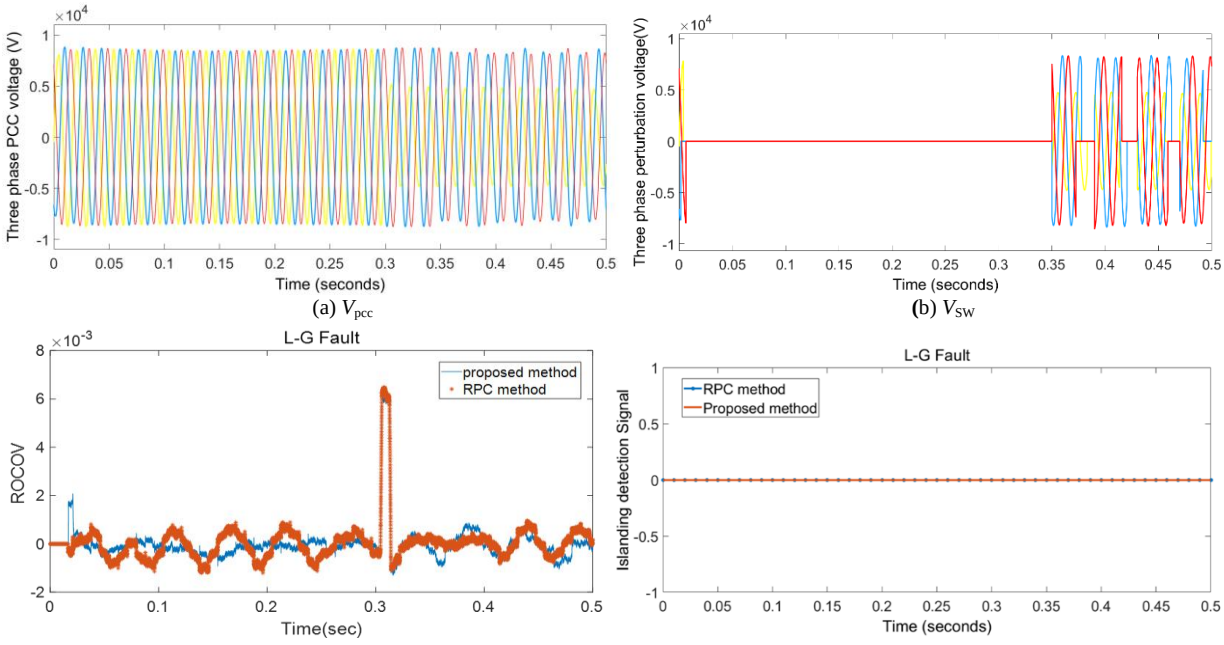

(a) V_{pcc} (b) V_{SW}

(c) ROCOV for the proposed method and RPC method. (d) Islanding detection signal

Fig. 11. Waveforms during L-G fault in the microgrid.

F. L-G Fault

One of the non-islanding events is a single-phase to ground fault that occurs at 0.3 s in line number 11-12 with R_f is equal to 1.5 Ω. This fault causes distortions in three-phase PCC voltage, as seen in Fig.11 (a). And the voltage of switched impedance during L-G fault is shown in Fig.11 (b).

During the L-G fault, the ROCOV of both methods is approximately similar, as can be seen from Fig. 11 (c). During the L-G fault in the RPC method, the actual value of the PCC voltage during islanding varies from the nominal PCC voltage. So, angle θ is participating in calculating the reactive power reference.

Table II Shows the L2 norm of θ for the L-G is greater than 527. At the same time, the Pearson correlation coefficient ρ, according to Table II, is greater than 0.3. As a result, both methods detect L-G fault correctly as a non-islanding event. Therefore, the islanding detection signal for both techniques equal zero in Fig.11 (d).

G. Islanding with Zero Power Mismatch

The islanding happens with zero power mismatch condition is implemented by opening the main circuit breaker in the 6-7 line at 0.3 s with zero power mismatch between the generation and the demand.

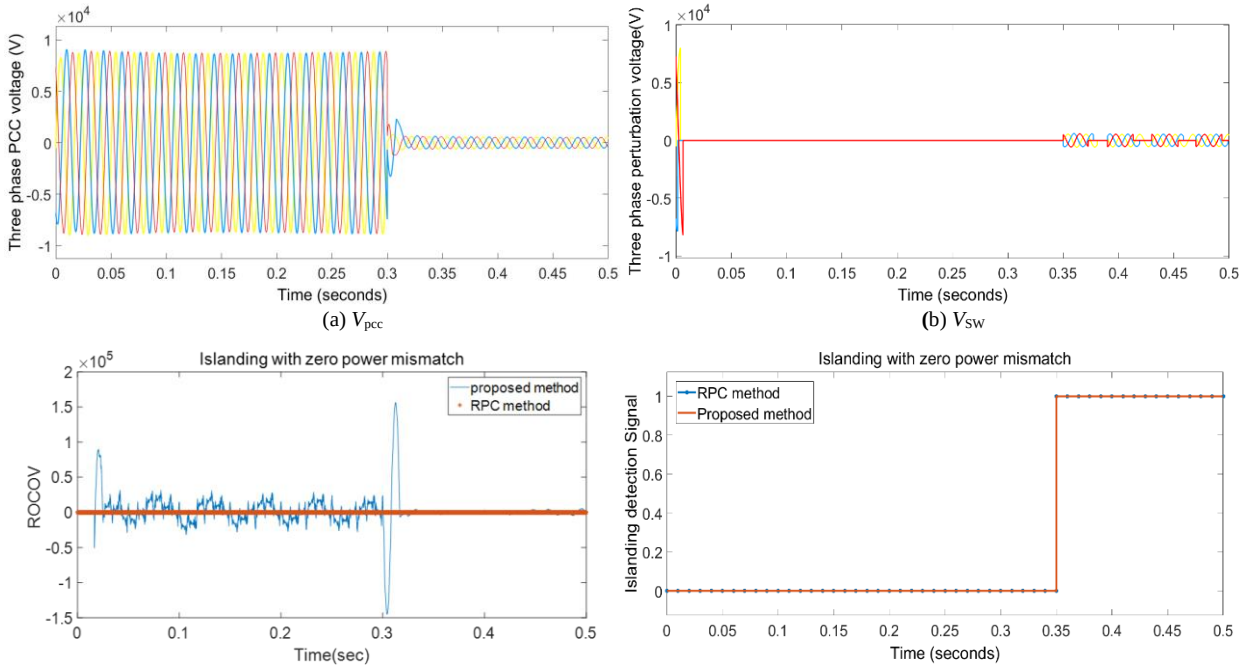

(a) V_{pcc} (b) V_{SW}

(c) ROCOV for the proposed method and RPC method (d) Islanding detection signal

Fig. 12. Waveforms during islanding with zero power mismatch.

After the main grid was disconnected, MG and PCC loads formed an island, and PCC voltage was no longer controlled by the main grid. As a result, when the main circuit breaker is opened at 0.3 s, the PCC voltage gets distorted with magnitude of 1Kv, as shown in Fig. 12 (a).

The voltage of switched impedance distorted when 5MVAR impedance is adjusted frequently from 0.35 s to 0.5 s due to the lack of voltage compensation from the main grid.

As shown from Fig. 12 (b), the three-phase voltage of injected impedance is periodic distorted voltage with voltage magnitude of 1 kV during the islanding from 0.3s to 0.5s.

ROCOV at PCC during islanding is a fluctuated value. The high value of ROCOV demonstrates significant changes in PCC voltage which indicates the islanding. Fig. 12 (c) illustrates the ROCOV of both methods during islanding with zero power mismatch. The straight line indicates the ROCOV of the proposed method, and the line marked with a star indicates the ROCOV of the RPC method. Islanding occurs at 0.3 s. ROCOV of the proposed method is higher than the ROCOV of the RPC method due to switched impedance. Therefore, the ROCOV of the proposed method illustrates significant changes in PCC voltage better than the ROCOV of the RPC method.

Since the actual value of the PCC voltage during islanding deviates from the nominal PCC voltage, angle θ is used to calculate the reference of the reactive power. Table II shows that the L2 norm for the islanding with zero power mismatch is less than 527.Therefore, the RPC approach detects islanding accurately. At the same time, the Pearson correlation coefficient is less than 0.3, as shown in Table II. As a result, the suggested method detects islanding correctly. The islanding detection signal for both procedures is equal, as illustrated in Fig. 12 (d).

V. Conclusion

The islanding fault is an unwanted phenomenon that threatens power system security and interrupts network operations can damage network and customer equipment, and endanger maintenance workers' lives. This paper proposed a new HIDM for a grid-connected microgrid with inverter-based and non-inverter-based sources. The voltage fluctuation injection method is developed using the Pearson correlation coefficient. Pearson correlation coefficient between the three-phase PCC voltage and three-phase voltage of switched impedance is used as a similarity measure to detect islanding. Normal operation grid-connected microgrid had the highest Pearson correlation coefficient.

On the other hand, the islanding operation had the lowest Pearson correlation coefficient. The obtained results demonstrated the efficiency of the proposed method compared with the RPC method over five different cases: Islanding with high power mismatch, islanding DG1, islanding DG2; capacitor switching, LLL fault, and L-G fault, islanding with zero power mismatch. In comparison, the RPC method detects LLL-fault incorrectly as an islanding event.

The proposed method can successfully differentiate between islanding and non-islanding events successfully without NDZs. Moreover, islanding can be detected in less than 0.20 s using the proposed method within the 2 s threshold stipulated in islanding detection standards such as the IEEE 1547 UL 1741 standards.

Therefore, the authors recommend implementing the proposed method on a practical system. The future scope of this work is to use an intelligent classifier for islanding detection to avoid the difficulty related to threshold value selection.

APPENDIX

TABLE AI: LINE DATA

Sending Bus	Receiving Bus	*R* (ohm)	*X* (ohm)
1	2	0.176	0.138
2	3	0.176	0.138
3	4	0.045	0.035
4	5	0.089	0.069
5	6	0.045	0.035
6	7	0.116	0.091
7	8	0.073	0.073
8	9	0.074	0.058
8	10	0.093	0.093
7	11	0.063	0.050
11	12	0.068	0.053
7	13	0.062	0.053

TABLE AII: LOAD DATA

No. bus	*P* (KW)	*Q* (KVAR)
1	0	0
2	890	468
3	628	470
4	1112	764
5	636	378
6	474	344
7	1342	1078
8	920	292
9	766	498
10	662	480
11	690	186
12	1292	554
13	1124	480

CONFLICT OF INTEREST

The authors declare no conflict of interest.

AUTHOR CONTRIBUTIONS

The first author conducted the research and wrote the paper. The second and third authors supervised the conducting of the research and review the paper.

ACKNOWLEDGMENT

The authors wish to thank African Union Commission (AUC). This work was supported by AUC through PAUSTI research grant.

REFERENCES

[1] S. Dutta, P. K. Sadhu, M. Jaya Bharata Reddy, and D. K. Mohanta, "Shifting of research trends in islanding detection method - a comprehensive survey," *Protection and Control of Modern Power Systems*, vol. 3, no. 1, pp. 1–20, 2018.

[2] M. Yousaf and T. Mahmood, "Protection coordination for a distribution system in the presence of distributed generation," *Turkish Journal of Electrical Engineering and Computer Sciences*, vol. 25, no. 1, pp. 408–421, 2017.

[3] J. S. Farkhani, M. Zareein, A. Najafi, R. Melicio, and E. M. G. Rodrigues, "The power system and microgrid protection—a review," *Applied Sciences (Switzerland)*, vol. 10, no. 22. pp. 1–30, Nov. 2020.

[4] A. Hirsch, Y. Parag, and J. Guerrero, "Microgrids: A review of technologies, key drivers, and outstanding issues," *Renewable and Sustainable Energy Reviews*, vol. 90. pp. 402–411, Jul. 2018.

[5] M. Hosseinzadeh and F. R. Salmasi, "Islanding fault detection in microgrids-a survey," *Energies*, vol. 13, no. 13, 2020.

[6] S. Beheshtaein, R. Cuzner, M. Savaghebi, and J. M. Guerrero, "A review on microgrids protection," *IET Generation, Transmission and Distribution*, vol. 13, no. 6, pp. 743–759, 2019.

[7] M. S. Kim, R. Haider, G. J. Cho, C. H. Kim, C. Y. Won, and J. S. Chai, "Comprehensive review of islanding detection methods for distributed generation systems," *Energies*, vol. 12, no. 5. pp. 1–21, Mar. 4, 2019.

[8] M. Suman and M. V. Kirthiga, "Unintentional islanding detection," in *Distributed Energy Resources in Microgrids: Integration, Challenges and Optimization*, Elsevier, 2019, pp. 419–440.

[9] S. Admasie, S. B. A. Bukhari, R. Haider, T. Gush, and C. H. Kim, "A passive islanding detection scheme using variational mode decomposition-based mode singular entropy for integrated microgrids," *Electric Power Systems Research*, vol. 177, Dec. 2019.

[10] W. Xu, G. Zhang, C. Li, W. Wang, G. Wang, and J. Kliber, "A power line signaling based technique for anti-islanding protection of distributed generators - Part I: Scheme and analysis," *IEEE Trans. on Power Delivery*, vol. 22, no. 3, pp. 1758–1766, 2007.

[11] G. Bayrak and E. Kabalci, "Implementation of a new remote islanding detection method for wind-solar hybrid power plants," *Renewable and Sustainable Energy Reviews*, vol. 58, pp. 1–15, May 2016.

[12] B. Dob and C. Palmer, "Communications assisted islanding detection contrasting direct transfer trip and phase comparison methods," in *Proc. 71st Annual Conference for Protective Relay Engineers*, 2018.

[13] K. Subramanian and A. K. Loganathan, "Islanding detection using a micro-synchrophasor for distribution systems with distributed generation," *Energies (Basel)*, vol. 13, no. 19, Oct. 2020.

[14] V. Muzik and V. Vajnar, "Frequency and Voltage stability assessment of a power system during emergency service states," in *Proc. IEEE Conference of Russian Young Researchers in Electrical and Electronic Engineering (EIConRus)*, 2018.

[15] M. Karimi, M. Farshad, Q. Hong, H. Laaksonen, and K. Kauhaniemi, "An islanding detection technique for inverter-based distributed generation in microgrids," *Energies (Basel)*, vol. 14, no. 1, Jan. 2021.

[16] C. R. Reddy, G. R. Reddy, B. S. Goud, N. Rajeswaran, and C. N. Kumar, "Passive islanding detection methods for integrated distributed generation system," *Journal of Power Technologies*, vol. 201, no. 3, pp. 127-134, 2021.

[17] D. Mlakic, H. R. Baghaee, and S. Nikolovski, "A novel ANFIS-based islanding detection for inverter-interfaced microgrids," *IEEE Trans. on Smart Grid*, vol. 10, no. 4, pp. 4411–4424, Jul. 2019.

[18] F. Ghalavand, B. A. Mohammadi Alizade, H. Gaber, and H. Karimipour, "Microgrid islanding detection based on mathematical morphology," *Energies (Basel)*, vol. 11, no. 10, Oct. 2018.

[19] G. P. Kumar and P. Jena, "Pearson's correlation coefficient for islanding detection using micro-pmu measurements," *IEEE Systems Journal*, vol. 15, no. 4, pp. 5078–5089, Dec. 2021.

[20] N. Gupta and R. Garg, "Algorithm for islanding detection in photovoltaic generator network connected to low-voltage grid," *IET Generation, Transmission and Distribution*, vol. 12, no. 10, pp. 2280–2287, May 2018.

[21] S. Yu and L. Yin, "Islanding detection method based on S transform and ANFIS," *Journal of Renewable and Sustainable Energy*, vol. 10, no. 5, Sep. 2018.

[22] S. C. Kim, P. Ray, and S. R. Salkuti, "Islanding detection in a distribution network with distributed generators using signal processing techniques," *International Journal of Power Electronics and Drive Systems*, vol. 11, no. 4, pp. 2099–2106, Dec. 2020.

[23] A. Rostami, A. Jalilian, S. Zabihi, J. Olamaei, and E. Pouresmaeil, "Islanding detection of distributed generation based on parallel inductive impedance switching," *IEEE Systems Journal*, vol. 14, no. 1, pp. 813–823, Mar. 2020.

[24] M. S. Rawat and S. Vadhera, "Evolution of islanding detection methods for microgrid systems," in *Optimizing and Measuring Smart Grid Operation and Control*, 2020, pp. 221–257.

[25] M. Seyedi, S. A. Taher, B. Ganji, and J. Guerrero, "A hybrid islanding detection method based on the rates of changes in voltage and active power for the multi-inverter systems," *IEEE Trans. on Smart Grid*, vol. 12, no. 4, pp. 2800–2811, Jul. 2021.

[26] B. K. Chaitanya, A. Yadav, M. Pazoki, and A. Y. Abdelaziz, "A comprehensive review of islanding detection methods," in *Uncertainties in Modern Power Systems*, Elsevier, 2021, pp. 211–256.

[27] A. Rostami, H. Abdi, M. Moradi, J. Olamaei, and E. Naderi, "Islanding detection based on ROCOV and ROCORP parameters in the presence of synchronous DG applying the capacitor connection strategy," *Electric Power Components and Systems*, vol. 45, no. 3, pp. 315–330, Feb. 2017.

[28] R. Bakhshi-Jafarabadi and M. Popov, "Hybrid islanding detection method of photovoltaic-based microgrid using reference current disturbance," *Energies (Basel)*, vol. 14, no. 5, Mar. 2021.

[29] A. Aref, M. Davoudi, F. Razavi, and M. Davoodi, "Optimal DG placement in distribution networks using intelligent systems," *Energy and Power Engineering*, vol. 4, no. 2, pp. 92–98, 2012.

[30] P. Schober and L. A. Schwarte, "Correlation coefficients: Appropriate use and interpretation," *Anesthesia and Analgesia*, vol. 126, no. 5, pp. 1763–1768, May 2018.

[31] H. Lin, K. Sun, Z.-H. Tan, C. Liu, J. M. Guerrero, and J. C. Vasquez, "Adaptive protection combined with machine learning for microgrids," *IET Generation, Transmission and Distribution*, vol. 13, no. 6, pp. 770–779, 2019.

[32] H. Davarikia, M. Barati, F. Znidi, and K. Iqbal, "Real-time integrity indices in power grid: a synchronization coefficient based clustering approach," in *Proc. IEEE Power and Energy Society General Meeting*, 2018.

[33] P. P. Mishra and C. N. Bhende, "Islanding detection scheme for distributed generation systems using modified reactive power control strategy," *IET Generation, Transmission and Distribution*, vol. 13, no. 6, pp. 814–820, 2019.

Nusiaba A. H. Hamed B.Sc. (Honors) in electrical and electronic engineering (power systems), University of Kassala, Sudan, 2017. She worked as a Teaching Assistant at University of Kassala for 3 years. She is a student M.Sc. at Pan African University Institute of Basic Sciences Technology and Innovation (PAUSTI) in the Electrical Engineering Department (Power Systems Option), Juja, Kenya.

George N. Nyakoe graduated in 1993 with a B.Sc. degree in Electrical and Electronic Engineering from the University of Nairobi. He received the M.Sc. and Ph.D. degrees in Electrical Engineering from Tottori University, Japan, in 2000 and 2003, respectively. He is currently a Professor at Jomo Kenyatta University of Agriculture and Technology and an adjunct professor at the Pan African University Institute for Basic Science, Technology and Innovation (PAUSTI), Kenya. His current research interests include control of power electronic systems, distributed generation integration and artificial intelligence applications.

Michael J. Saulo is the Registrar for Partnership, Research and Innovation at Technical University of Mombasa (TUM) and a Senior Lecturer in Electrical Engineering. He has been involved in numerous research activities and conferences on the themes of Sustainability, Clean Energy, Climate Change, and their connection and consequences to society. He is the founder and Director of the Renewable Energy and Climate Change Research Centre (RECCREC) in TUM. He is a seasoned researcher with over 70 publications in refereed Journal.